The Open Civil Engineering Journal

Content list available at: https://opencivilengineeringjournal.com

RESEARCH ARTICLE

Suitability of Using LA Abrasion Machine for the Nano Manufacturing of Palm Oil Fuel Ash and Incorporating in Mortar Mixture

Yu Xuan Liew[1], Ramadhansyah Putra Jaya[1] and Siew Choo Chin[1,2,*]

[1]*Faculty of Civil Engineering Technology, Universiti Malaysia Pahang Al-Sultan Abdullah, Gambang 26300, Pahang, Malaysia*
[2]*Center for Research in Advanced Fluid and Processes, Fluid Centre, Universiti Malaysia Pahang Al-Sultan Abdullah, 26300 Gambang, Pahang, Malaysia*

Abstract:

Background:

In order to enhance the properties of palm oil fuel ash-based mortar, researchers have explored the concept of reducing palm oil fuel ash (POFA) to a nanoscale. While previous studies have utilized ball milling machines with high grinding speed to achieve nano-scale POFA, the Los Angeles abrasion machine, which is more readily available and has a slower grinding speed, has been rarely employed.

Objective:

The study aimed to investigate the suitability of using a Los Angeles abrasion machine with a low grinding speed to produce nano palm oil fuel ash. This paper also provides a comparison of the effect of using the nano POFA with different particle sizes within the range of 982 to 150 nm on the mortar's flowability and compressive strength.

Methods:

To produce nano-size palm oil fuel ash using the Los Angeles abrasion machine, the received palm oil fuel ash was thermally treated and ground using a Los Angeles abrasion machine with varying grinding periods. The grinding process parameters were kept constant, but second grinding periods of 50,000, 80,000, and 110,000 cycles were introduced. All three types of nano palm oil fuel ash were analyzed for their physical properties, chemical properties, morphology, and mineralogy. Furthermore, these nano palm oil fuel ashes were incorporated into a designed mortar mix along with micro palm oil fuel ash. The mortar's fresh properties and compressive strength at different curing ages were observed and analyzed. The relationship between various factors, such as the replacement rate of micro, nano palm oil fuel ash, the grinding cycles of nano POFA, and the corresponding responses, specifically the compressive strength at different curing ages, was analyzed and explained using the response surface methodology.

Results:

The 110k cycle nano palm oil fuel ash had a smaller particle size of 103.1 nm, while a particle size of 529 nm and 325 nm was found in the 50k and 80k cycle nano palm oil fuel ash. In terms of the combination of micro and nano palm oil fuel ash in the mortar, increasing the dosage of nano palm oil fuel ash contributed to improvements in flow diameter and compressive strength. However, the opposite trend was observed with micro palm oil fuel ash. The optimal mix design for the combination involved using 10% micro and 2 to 3% nano palm oil fuel ash. This composition led to an improvement rate of 7.9%, 1.48%, and 4.6% in compressive strength at 7, 28, and 90 days, respectively. While, the response surface methodology's numerical optimization also supported the use of a similar combination. However, it additionally recommended employing the 50,000-cycle nano palm oil fuel ash in the mortar for earlier curing stages, while the 110,000-cycle nano palm oil fuel ash was suggested for later curing stages.

Conclusion:

Los Angeles abrasion machine could be utilized to produce nano palm oil fuel ash with a particle size up to 103 nm with the aid of designed parameters. In this mortar mix design, the impact of a small variance in nano palm oil fuel ash's particle size was trivial compared to the replacement rate of micro palm oil fuel ash on the mortar's compressive strength.

Keywords: POFA, Nano, Micro, LA abrasion machine, RSM, Compressive strength.

Article History	Received: August 03, 2023	Revised: September 06, 2023	Accepted: September 15, 2023

1. INTRODUCTION

To achieve the 1.5 to 2°C stabilization in global temperature rise that has been agreed upon by the international community during the COP21 event in Paris, the approach of reducing CO_2 emission to net zero was implemented worldwide, especially in the CO_2-intensive sectors [1, 2]. The cement industry plays one of the important roles responsible for global CO_2 emissions up to 8% annually generated from the decomposition of limestone and fossil fuel combustion during cement production [3, 4]. Thus, several efforts to reduce carbon emissions in the cement industry have been made, including utilizing supplementary cementitious materials (SCMs) in the concrete mix as cement replacement [5, 6]. The SCMs that are either an industry by-product or natural materials have pozzolanic properties and, thus, the use of SCM for cement substitution in the concrete mix has led to improvements in concrete's late hardened properties, durability, and a reduction in heat of hydration [7 - 9].

Palm oil fuel ash (POFA) has a high content of silica, which is responsible for the pozzolanic reaction, and can be used as a cement replacement. It is a byproduct that is generated from the combustion of palm oil waste during palm oil extraction with an expected annual production rate of up to 10 to 12 million tons [10 - 12]. Turning it into cement replacement seems to be a better choice rather than disposing and it becoming a potential environmental pollutant. The POFA has been reported to contain high unburned carbon content and non-uniform physiochemical properties, which result in affecting the fresh properties and engineering properties of the concrete incorporating raw POFA beyond the optimum replacement rate [13 - 15]. Hence, the effort to reduce the fineness of SCM particles has been made to improve the SCM's pozzolanic reactivity, which has been found to later enhance both the fresh and engineering properties of concrete [16, 17]. Nano-scale POFA has been extensively utilized as a cement replacement to enhance POFA cement mixtures, and reported positive results. In terms of fresh properties, the nano POFA-based concrete exhibited greater workability than the control sample. Hassan *et al*. [18] and Tang [19] reported that the utilization of nano POFA with the particle size range of 20 to 90 nm improved the slump value of concrete up to 7% than the control at the dosage of 3%. This can be attributed to the low unburned content of nano POFA and its better lubrication effect [19 - 21]. In terms of hardened properties, the nano POFA-based cement mixtures showed significant improvements ranging from 2% to 35% across all curing ages, surpassing the performance of micro and raw POFA at a higher optimum replacement rate [22 - 24].

The production of nano-structured POFA is predominantly achieved through the use of a high-energy ball milling machine, with the reported particle size ranging from 20 nm to 150 nm [20, 22, 25, 26]. Unfortunately, less detail regarding the nano-structuring process of the nano POFA has been provided in the abovementioned papers. Hassan *et al*. [18] used the high energy ball milling machine with a capacity of 0.032 m^2 and a combination of various diameters of steel balls to grind the POFA from micro to nanoscale in 5 hours. In contrast, Rajak *et al*. [27], who used the ceramic ball milling machine to produce the nano POFA in the size of 20 to 90 nm, reported a grinding time of 30 hours. Rizal *et al*. [28] further explored the optimum grinding conditions to produce nano POFA more efficiently by using a high-energy ball milling machine, and concluded that the optimum parameters were using the iron ball size of 20 mm diameter, grinding time of 24 hours, and milling speed of 100 rpm. Compared to those authors who used the high-energy ball milling machine with a faster grinding speed, only Hamada *et al*. [29] produced the nano POFA with a particle size of 982 nm by using the Los Angeles (LA) abrasion machine, which had a lower grinding speed.

It can be concluded that factors, such as the weight ratio of steel ball to input POFA, ball diameters, grinding time, and grinding speed, impact the efficiency of producing nano POFA. Designing a grinding parameter with a longer grinding time, fixed weight ratio of steel balls to feed POFA, a combination of various diameter steel balls, and lower grinding speed might improve the grinding efficiency. Most of the past researchers have utilized high-energy ball milling, which grinds the POFA at a higher grinding speed, but Rizal *et al*. [28] recommended that using a lower grinding speed might give better grinding efficiency. The author warned that the high temperature produced during the machine operation might deform the particle properties as well as increase the average crystal size of the feed material. Moreover, the conventional ball milling machine with a bigger capacity usually has a slower grinding speed. However, the usage of a ball grinding machine with a lower grinding speed, such as an LA abrasion machine, in producing nano POFA is limited, and the produced POFA's particle size is not in the range of nanoscale. Hence, improving the grinding parameters of low-speed grinding machines to produce nano-scale POFA is worth trying. Apart from that, the nano POFA with particle size ranging from 150 nm to 985 nm has rarely been discovered in past studies, especially the particle properties and impact on cementitious mixture's properties.

Mathematical and statistical analyses, such as response surface methodology (RSM), are frequently employed in the investigation of cement mix design for experimental design optimization [30 - 32]. This optimization process is crucial for selecting an appropriate mix design that fulfills specific concrete requirements. Compared to conventional optimization methods, such as trial and error or single-variable methods, RSM offers a more efficient approach that saves time and resources [33]. Unlike conventional methods, the RSM offers appropriate solutions considering the relationship between various factors and responses. This makes it an ideal tool for determining the optimum response and optimum condition from multiple responses [34].

Thus, this work has further explored the suitability of utilizing the Los Angeles abrasion machine that has a lower grinding speed of 33 rpm for producing the nanoscale POFA. After that, this work has investigated the physiochemical properties of the nano POFA with the expected particle size in the range of 982 nm to 150 nm as well as the substitution effect

* Address correspondence to this author at Faculty of Civil Engineering Technology, Universiti Malaysia Pahang Al-Sultan Abdullah, Gambang 26300, Pahang, Malaysia; Tel: +6094316165; E-mail: scchin@ump.edu.my

of the nano POFA on the mortar's properties. The grinding parameters have been modified based on the work of Hamada *et al*. [35] and the recommendation from Rizal *et al*. [28], incorporating a different iron ball size, a fixed weight ratio of iron ball to feed, and testing of different grinding cycles. Following the grinding process, the nanoscale POFA samples produced with varying grinding cycles underwent physical, chemical, and morphological property tests. Subsequently, both the nanoscale POFA and micro POFA were incorporated as cement replacements in mortar mix designs. The fresh properties and hardened properties of the resulting mortars were evaluated at different curing ages. Lastly, the RSM was implemented during data analysis to determine the impact of various factors, including the different grinding cycles of nano POFA, on the hardened properties of mortar.

2. MATERIALS AND METHODS

2.1. Micro and Nano Scale POFA Preparation

2.1.1. Micro POFA

The raw POFA was collected from the palm oil mill located at Gambang, Pahang, Malaysia, and kept in the Concrete Lab University Malaysia Pahang. POFA was dried in an oven with a temperature of 100 ± 5 °C for one day to remove the excess water moisture in the ash before being further processed. Next, the dried raw POFA was sieved through the 300 µm sieve to remove the excess unburnt carbon. To further reduce the sieved POFA's particle size to less than 45 µm, the dried sieved POFA was ground in the LA abrasion machine with a grinding speed of 33 rpm for 10,500 cycles with a dosage of 3 kg per round. To ensure that the particle size of the ground POFA was less than 45 µm, around 100 g of ground POFA was obtained after each round of grinding and sieved through the 45 µm sieve. Each batch of ground POFA was kept only if the passing rate of the ground POFA was more than 90% passing through the 45 µm sieve according to the standard, ASTM C618-2019. The ground POFA was burnt in the furnace at the temperature of 600°C for 2 hours to fully remove the unburned carbon in it. Until this stage, this POFA was marked as micro POFA.

2.1.2. Nano POFA

To prepare nanoscale POFA, the micro POFA was ground in the same LA machine again, but with different grinding parameters. A constant weight ratio of iron steel ball to feed was maintained at 10:1, while there were two types of iron ball diameter used, which were 50 mm and 20 mm. The mass of the feed POFA was 1.5 kg, while the total weight of the steel was 15kg. Finally, the grinding time was designed as 50,000, 80,000, and 110,000 cycles. The grinding cycles, 50,000, 80,000, and 110,000 are denoted as 50k, 80k, and 110k in this paper. The preparation process for 50k cycles of nano POFA is presented in Fig. (**1**).

Fig. (1). Preparation flow of the 50k cycle nano POFA.

2.2. POFA Characteristics

2.2.1. Physical Properties

The physical properties of POFA were evaluated in terms of the specific surface area and particle size. The specific surface area of POFA was determined with the Brunauer–Emmett–Teller (BET) analysis. The preliminary checking of the particle size of POFA was carried out by using a dry sieve to fulfill the particle size requirement of the ASTM C618-2019 standard. Later, the actual particle size as well as the particle size distribution of POFA were tested by the particle size analyzer.

2.2.2. Loss of Ignition (LOI)

ASTM D7348-21 standard was referenced to measure the LOI value of all types of POFA. Around 1 ± 0.5 g of POFA was weighed and placed in the oven-dried crucible. Then, the POFA with the crucible was dried in the oven for an hour, and the weight of the dried POFA and crucible was recorded. Next, the POFA was placed in a desiccator to let it cool. The next step was heating the samples in a furnace for 2 hours at a temperature of 950 ºC. The fired sample was then cooled to room temperature in a desiccator, and the weight was recorded. The weight loss at this stage was taken as the LOI value.

2.2.3. Chemical Properties, Mineralogy, and Morphology of POFA

The chemical properties of POFA were examined through X-ray fluorescence (XRF). X-ray diffraction (XRD) was carried out on the POFA to test the mineralogy of POFA. The start and end angle of the XRD analysis was 2 degrees and 90 degrees, respectively, while the step size was 0.05 degrees per minute. The morphology of the POFA was determined through scanning electron microscopy (SEM).

2.3. POFA as Cement Replacement in Mortar Mix

2.3.1. Cement

The type 1 Ordinary Portland Cement (OPC) that was obtained from a local supplier was used in this experiment. The specification of the OPC followed the standard. The cement was produced by a local cement manufacturer by following the MS EN197-2014 CEM I 52.5 N.

2.3.2. Aggregate

The river sand was used as fine aggregate with a size between 1.18 mm to 0.6 mm by following the ASTM C778-2021 standard.

2.3.3. Water

Portable tap water was used in the cement paste and mortar mix design where the water was supplied by Jabatan Bekalan Air Pahang. The used water in the mix design was required to be clean and unpolluted to avoid disturbing the cement hydration process and curing process.

2.3.4. Mortar Mix Design

The preparation and mixing of mortar were carried out in accordance with the ASTM C109-2021 standards. The mortar was designed to have a cement-to-sand ratio of 1:2.75, while the cement-to-water ratio was 1:0.485. The mold size for the compressive test was 50 mm x 50 mm x 50 mm (L x W x H). The replacement rate of the micro POFA and nano POFA is presented in Table **1**. The mortar was removed from the mold after one-day casting and subjected to water curing until 7-, 28- and 90-day curing ages.

2.4. Fresh and Hardened Properties of Mortar

2.4.1. Fresh Properties

The flowability of the mortar has been studied to explore the impact of introducing the combination of nano and micro POFA on the mortar mix design. The flow of fresh control mortar was controlled at 110 ± 5 of the flow table by referring to the ASTM C109-2021 standard.

2.4.2. Hardened Properties

A compressive strength test of mortars from each POFA specimen was conducted in triplicate at the 7, 28, and 90-day curing age in accordance with ASTM C109-2021 by using the universal testing machine. Later, the interaction between the mortar mix design, grinding cycles of nano POFA, and the hardened properties of mortar at different curing ages has been expressed with the aid of statistical test setup and response surface methodology (RSM).

Table 1. Mortar mix design.

Mix No.	Micro POFA Replacement Rate (%)	50k Cycles Nano POFA Replacement Rate (%)	80k Cycles Nano POFA Replacement Rate (%)	110k Cycles Nano POFA Replacement Rate (%)
M0	0	0	0	0
M10N1	10	1	1	1
M10N2	10	2	2	2
M10N3	10	3	3	3
M20N1	20	1	1	1
M20N2	20	2	2	2
M20N3	20	3	3	3
M30N1	30	1	1	1
M30N2	30	2	2	2
M30N3	30	3	3	3

3. RESULTS AND DISCUSSION

3.1. Properties of POFA

3.1.1. Physical Properties

The physical properties of three types of nano POFA are presented in Table **2**. It can be observed that the 50k cycle nano POFA had a particle size of 529.0 nm; while increasing the grinding cycle to 110k, the particle size of nano POFA decreased to 103.1 nm. This demonstrates the potential of using the Los Angeles abrasion machine to produce nano POFA by manipulating the grinding parameters. In terms of specific surface area, the 110k cycle nano POFA demonstrated the highest value, indicating a larger surface area per unit mass. On the other hand, the 50k cycle nano POFA had a lower specific surface area, aligning with the observed particle size trend. All types of nano POFA had a greater specific surface area than the reported nano POFA, only having a value of 1.962 m^2/g for the 982 nm POFA and 3 m^2/g for the 100 to 150 nm nano POFA [36, 37].

Table 2. Physical properties of various grinding cycles of nano POFA.

Properties	50,000 Cycles Nano POFA	80k Cycles Nano POFA	110k Cycles Nano POFA
Diameter, D_{50} (nm)	529.0	325.0	103.1
Specific surface area (m^2/g)	5.81	5.92	5.99

Table 3. List of LOI of all types of POFA.

Type of POFA	LOI Value (%)
Raw POFA	28.13
Sieved POFA	10.85
Ground POFA	14.07
Micro POFA	2.54
50k cycle nano POFA	5.03
80k cycle nano POFA	4.34
110k cycle nano POFA	5.61

3.1.2. Loss of Ignition (LOI)

The POFA's LOI percentage reflects its unburnt carbon content, which later impacts the properties of cement mixture containing POFA as cement replacement [38, 39]. Chen *et al*. [40] and Phethany [41] found that the cement mixture having the lower LOI percentage of SCM exhibited a lower demand for the superplasticizer, shorter setting time at a constant substitution rate, and slightly impact its hardened properties. Table **3** presents the LOI value of various types of POFA. The raw POFA that was obtained from the palm oil mill had a high carbon content, where the LOI value reached 28.13%, which was far exceeding the limit stated in ASTM C618. After being sieved, ground, and thermally treated in the electric furnace at the temperature of 600°C for 2 hours, the LOI value of the micro POFA successfully reduced to 2.54%, which was lower than the limit set in the standard, and the reduction of POFA's LOI value aligned with other studies that have carried out thermal treatment [20, 38, 42]. However, the second grinding of micro POFA in the LA abrasion machine for the nano-structuring process led to the increment in the LOI value of all nano-scale POFA, but the LOI value of all nano POFA was still below 6%.

3.1.3. Chemical Properties of POFA

The content of chemical components, especially the minimum content of the sum of Al_2O_3, SiO_2, and Fe_2O_3 is stated in the standard ASTM C618. It can be found that the raw POFA not only had a high content of carbon, which was represented by the LOI value, but its silica content has also been found to be very low, *i.e*., only 13.7%, as reported in Table **4**. After being thermally treated and with reducing particle size, as the carbon has been removed from the ash, the content of Al_2O_3, SiO_2, and Fe_2O_3 in micro POFA and 80k cycle nano POFA was found to increase significantly, and the sum of those three components was reported at 70.96% and 75.38%, respectively, which exceeded the minimum requirement listed in the standard. A similar improvement has been reported earlier [22, 38] using the thermal treatment and grinding methods to enhance the content of Al_2O_3, SiO_2, and Fe_2O_3.

Table 4. List of chemical properties of all types of POFA.

Chemical Component (%)	Raw POFA	Sieved POFA	Micro POFA	80k Cycle Nano POFA
MgO	1.90	2.99	2.96	2.68
Al_2O_3	0.69	2.28	6.36	7.08
SiO_2	13.7	32.1	58.0	58.6
SO_3	2.19	1.14	1.58	1.02
K_2O	8.67	7.27	9.49	8.01
CaO	3.29	7.28	9.03	8.04
Fe_2O_3	1.34	3.50	6.60	9.70
Sum of Al_2O_3, SiO_2, and Fe_2O_3	15.73	37.88	70.96	75.38

3.1.4. Mineralogy of POFA

Micro POFA and 110k cycles nano POFA had a similar trend in the XRD result of micro POFA, as shown in Fig. (**2**), and the major mineral phase detected was the quartz. Besides that, a hump peak was found between 19 to 36.5 in both types of POFA, which indicated the low crystallinity of the micro and nano POFA. This hump peak of the sample's XRD result found in this research aligned with that reported earlier [22, 36, 38], where the hump was found at a degree ranging between 15° to 40°. The second grinding process was found to decrease the peak intensity of 110k nano POFA, which was 27.8% less than the peak intensity of micro POFA. A similar decrement of peak intensity in SCM's XRD result has been reported previously [43, 44] due to the grinding process, and this reduction indicated the reduction in crystallinity of quartz to a finer size. This was unlike the XRD result reported in a previous study [18], where the peak intensity of the nano POFA increased after being ground from micro to nanoscale in the high-energy ball milling machine. This increment aligned with the warning suggested in another work [28] due to the high grinding speed, which later increased the crystal size of quartz.

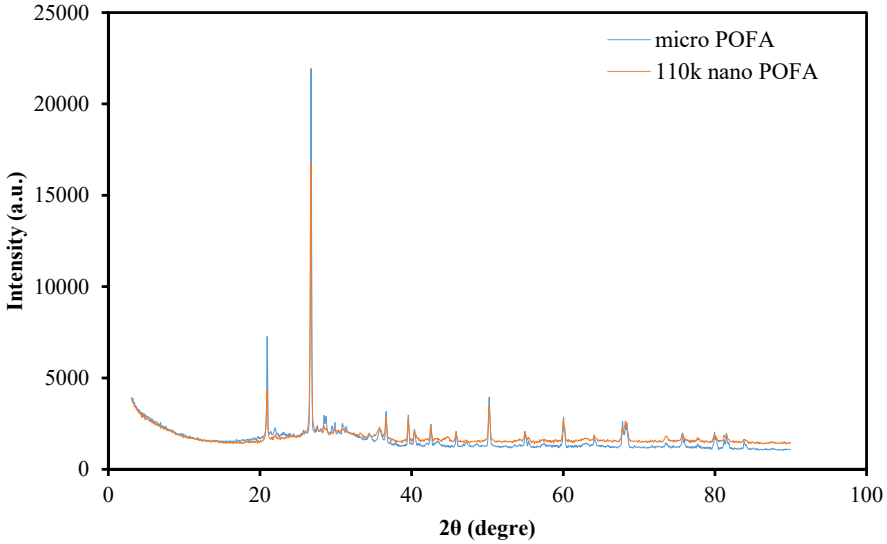

Fig. (2). Combined XRD result of micro and 110k cycles nano POFA.

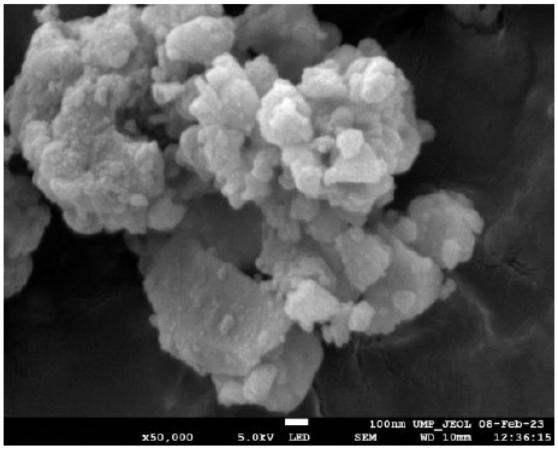

Fig. (3). 50k cycle nano POFA's morphology.

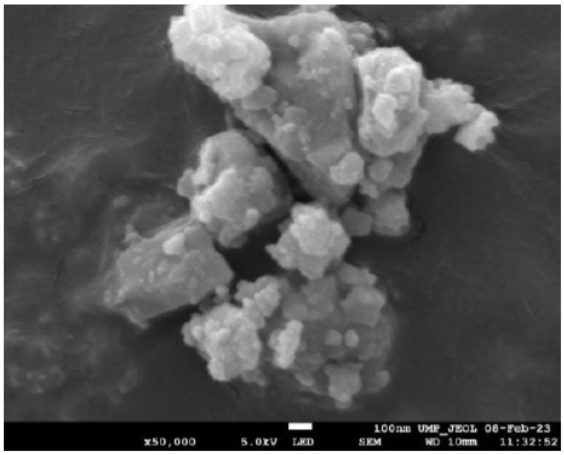

Fig. (4). 80k cycle nano POFA's morphology.

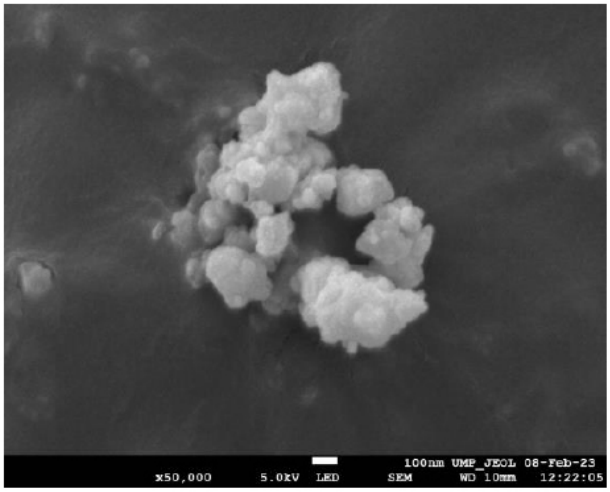

Fig. (5). 110k cycle nano POFA's morphology.

3.1.5. Morphology of POFA

Figs. (**3** - **5**) present the morphology of the 50k cycles, 80k cycles, and 110k cycles nano POFA. It was found that all three types of nano POFAs' particles tended to be aggregated with other particles and formed a bigger particle, which was similar to the result reported by Wi *et al*. [36]. Apart from that, the 50k cycle nano POFA particles had an angular shape with more edges, but the 80k cycles nano POFA had an angular shape with fewer edges than the 50k cycles. The 110k cycles nano POFA's particle was between angular and circular. Comparing the particle size among these three types of nano POFA, the 110k cycles nano POFA's particle seemed smaller compared to others, according to the result of the particle size analyzer.

3.2. Fresh Properties of Mortar Containing POFA

The flowability of the mortar was assessed to examine the effects of different combinations of micro and nanoscale POFA as partial cement replacements. The flow diameter is presented in Table **5**. It is evident that increasing the dosage of micro POFA had a greater impact on the flow diameter compared to increasing the dosage of nano POFA or the number of grinding cycles for nano POFA. When the dosage of micro POFA was increased to 30% in the mortar mix, the flow diameter decreased, compared to the mix with 10% micro POFA and the control sample. On the other hand, incorporating higher dosages of nano POFA, regardless of the grinding cycles, resulted in an improvement in the flow diameter of the mortar, particularly when combined with higher dosages of micro POFA (20% and 30%). This trend in the improvement of flow diameter aligns with the findings of previous studies [19, 20, 45]. The enhanced flow diameter in mortars containing 20% to 30% micro POFA can be attributed to the contribution of the fine particles of nano POFA. Due to its very fine particle size and lower specific gravity compared to OPC, nano POFA particles can adhere to the cement particles, which are negatively charged, preventing flocculation and agglomeration. As a result, the cement particles disperse more evenly, allowing for less water entrapment [26, 45]. Hamada *et al*. [46] and Zeyad *et al*. [38], who used fine POFA with the particle size of 2.06 μm and 0.982 μm as cement replacement in their concrete mix design, also reported an increment in workability of concrete as the replacement rate increased. The addition of fine POFA, with its lower specific gravity and finer particle size, increased the binder volume, improving coating, lubrication effects, and filling the voids between aggregates [47].

Table 5. Flow diameter of mortar.

Mix No.	50k Cycles Nano POFA	80k Cycles Nano POFA	110k Cycles Nano POFA
M0	120	120	120
M10N1	115	120	120
M10N2	122	120	118
M10N3	120	115	120
M20N1	113	115	120
M20N2	115	113	114
M20N3	120	120	120
M30N1	115	113	115
M30N2	118	116	119
M30N3	121	120	124

The LOI value of the three nano POFA samples was observed to be higher than that of the micro POFA, as well as the LOI values reported in previous studies ranging between 0.09% to 4.62% [21, 40, 46, 48]. However, these LOI values were still within the limits specified in ASTM C 618. Interestingly, the mortar's flow diameter showed a slight increase with increasing dosage of nano POFA, but the opposite trend was observed with increasing substitution rate of micro POFA. This suggests that the particle size of POFA has a greater impact on the flowability of the mortar compared to the LOI value. When comparing the effects of different grinding cycles on the flowability of the mortar, it was found that the 110k cycles nano POFA provided slightly better improvement compared to the 50k and 80k cycles. However, overall, the difference between the grinding cycles was not significant. Therefore, it can be concluded that in this experiment, the optimum dosage of nano POFA was more crucial in improving the fresh properties of the mortar compared to the grinding cycles and LOI value.

3.3. Hardened Properties of Mortar Containing POFA

Compressive strength is the utmost important parameter for evaluating the properties of cement-based material at different curing ages. Hence, this parameter has been utilized for assessing the impact of mix design and the grinding cycle on the mortar mix that was partially replaced by micro and nano POFA. Tables **6** - **8** present the compressive strength of mortar that contained various combinations of micro and three levels of grinding cycles of nano POFA, while Figs. (**6** - **8**) present the trends of various mortars' compressive strength at the curing ages of 7, 28, and 90 days.

Mortar that contained 10% micro POFA and 2% to 3% nano POFA without considering the impact of grinding cycles performed better than other combinations of micro and nano POFA. Further increasing the micro POFA replacement rate only led to a reduction in compressive strength at all curing ages. On the other hand, increasing the dosage of nano POFA despite the grinding cycles was found to improve the compressive strength of mortar that was substituted by a different rate of micro POFA at all curing ages. At the early curing age of 7 days, the mortar that contained 10% micro POFA and 2 to 3% nano POFA had higher compressive strength than the control in the range of 5.96 to 7.9%. While at the curing ages of 28 and 90 days, the M10N2-3 mortar had a relatively higher compressive strength of 1.48% and 4.6%, respectively, than the control. M20 mortar that contained 2 to 3% nano showed a reduction in compressive strength of 5%, 14%, and 6.07%, than the control at the ages of 7, 28, and 90 days. Compared to the M20, M10 mortar, and control, the M30 mortar exhibited a higher reduction in compressive strength, where a reduction rate of 14%, 12%, and 10% was found at the respective curing ages.

The inversely proportional trend between the substitution rate of micro POFA and the mortar's compressive strength, especially at the early curing age, has also been reported previously [22, 24, 36, 47, 49]. The micro POFA, which had a more porous particle, absorbed more water, and thus reduced the free water content for cement hydration; as the dosage of micro POFA increased, more water was absorbed and led to a higher reduction in cement mixture [20, 46]. In addition, increasing the replacement rate of SCM reduced the portion of cement at the same time. This led to the dilution of cement, where a lesser amount of calcium hydroxide (CH) was produced from the hydration process, while the CH was needed for the pozzolanic reaction. Hence, a lower quantity of the pozzolanic product, CSH gel, was produced and caused a reduction in the pozzolan-cement-based mixture's compressive strength with the replacement rate that exceeded the optimum rate [22, 49, 50]. Unlike the micro POFA, a positive increment trend was found in the compressive strength of mortar as the dosage of nano POFA increased. The finer particles of nano POFA demonstrated better pozzolanic reactivity as well as pore filling effect in the cement mixtures [22, 24]. Therefore, utilizing the nano POFA at the dosage of 3% incorporating 10% micro POFA as cement replacement in mortar led to an increment in mortar's compressive strength in the range of 6.4% to 7.6% at 7 days, 0.73% to 1.47% at 28 days, and 2.75% to 4.6% at 90 days.

There was a trivial difference found in the mortar's compressive strength at all curing ages when the three types of nano POFA were used. At the 7-day curing age, the mortar that contained 50 cycles nano POFA exhibited the highest compressive strength, followed by 80k cycles nano POFA, and the 110k cycles nano POFA had the lesser compressive strength. However, the trend changed at 28 and 90 days, where the 110k cycles nano POFA's mortar performed better than the others, and the 50k cycles nano POFA's mortar came second. This can be attributed to the particle size of various types of nano POFA, where the 110k cycle nano POFA had the finest particle. Hence, the 110k nano POFA-based mortar performed better than the 50k and 80k nano POFA mortar at late curing ages. In addition, the slower strength development of the 110k nano POFA than 50k nano POFA at ealier curing age may be due to the higher LOI value of 110k nano POFA and this led to a slower pozzolanic reaction.

Table 6. Mortar's compressive strength at 7 days.

Mix No.	50k Cycles Nano POFA	80k Cycles Nano POFA	110k Cycles Nano POFA
M0	40.74	40.74	40.74
M10N1	38.50	38.33	37.32
M10N2	46.37	43.96	43.17
M10N3	43.34	43.79	43.83
M20N1	39.06	36.83	38.77
M20N2	39.05	39.70	38.06
M20N3	38.39	39.05	39.76

(Table 6) contd.....

Mix No.	50k Cycles Nano POFA	80k Cycles Nano POFA	110k Cycles Nano POFA
M30N1	35.83	35.28	35.25
M30N2	35.51	35.05	36.03
M30N3	36.10	34.17	33.57

Table 7. Mortar's compressive strength at 28 days.

Mix No.	50k Cycles Nano POFA	80k Cycles Nano POFA	110k Cycles Nano POFA
M0	56.93	56.93	56.93
M10N1	53.99	53.00	55.63
M10N2	57.38	54.37	57.35
M10N3	57.77	57.38	55.12
M20N1	48.44	49.72	48.14
M20N2	49.25	48.62	50.30
M20N3	49.57	45.26	48.57
M30N1	42.07	44.15	46.96
M30N2	48.95	51.56	48.45
M30N3	50.54	50.70	51.17

Table 8. Mortar's compressive strength at 90 days.

Mix No.	50k Cycles Nano POFA	80k Cycles Nano POFA	110k Cycles Nano POFA
M0	59.62	59.62	59.62
M10N1	58.11	58.54	59.99
M10N2	60.61	58.39	60.09
M10N3	61.26	59.62	62.36
M20N1	53.50	53.14	54.48
M20N2	56.34	56.01	56.74
M20N3	55.15	53.18	54.40
M30N1	51.84	52.11	51.18
M30N2	52.69	52.19	57.69
M30N3	52.32	54.54	55.24

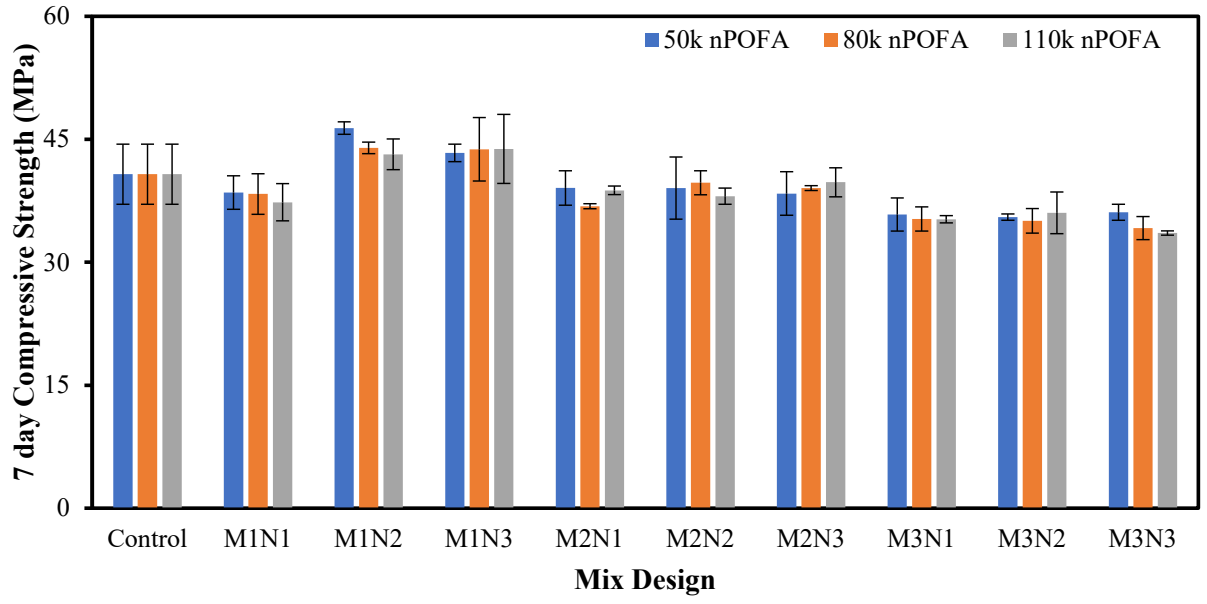

Fig. (6). Compressive strength of all mortars at the curing age of 7 days.

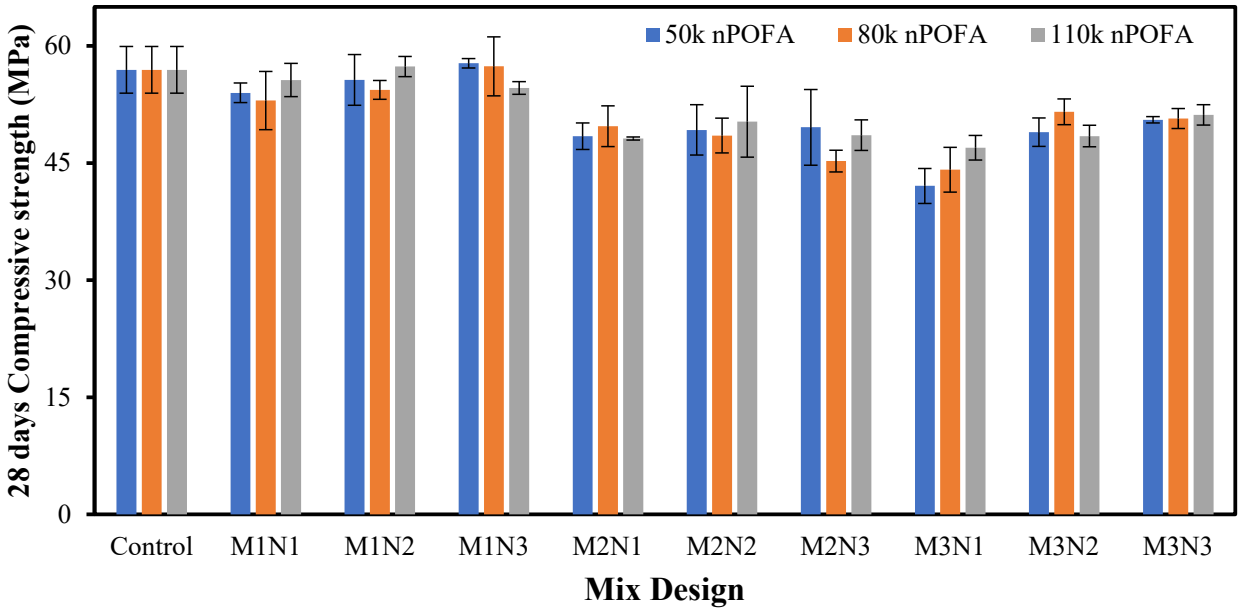

Fig. (7). Compressive strength of all mortars at the curing age of 28 days.

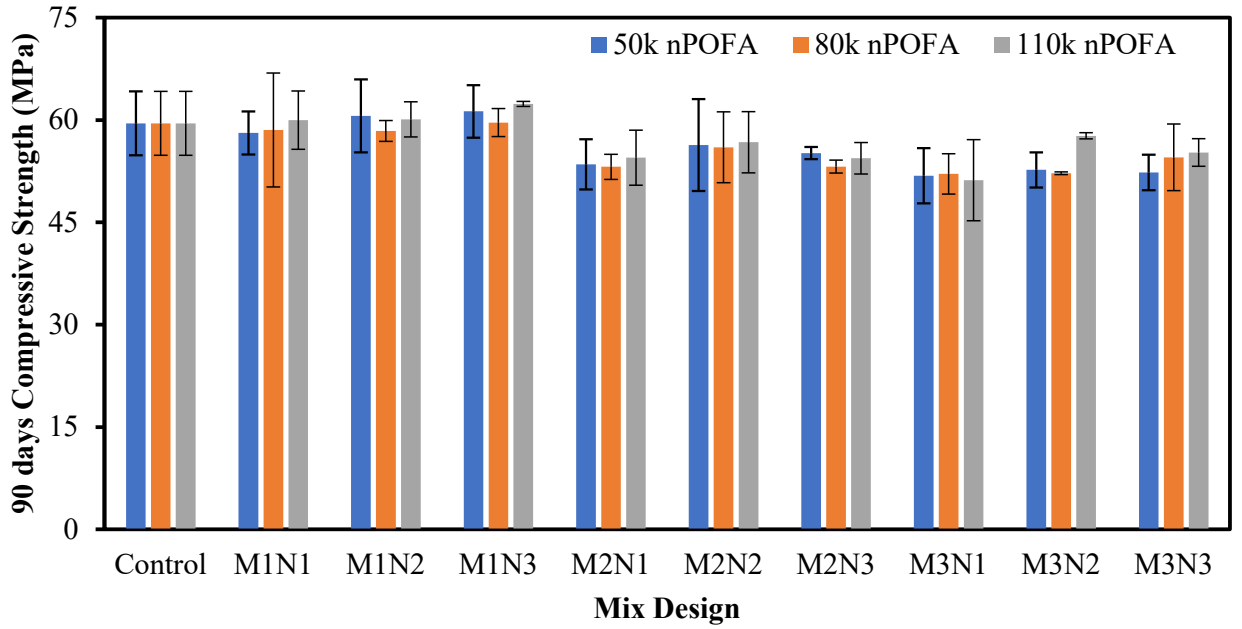

Fig. (8). Compressive strength of all mortars at the curing age of 90 days.

3.3.1. Analyzing Factor-Response Relationship by Using Response Surface Methodology (RSM)

The RSM computed an equation that described the relationship between the factors and responses based on coded factors, as summarized in Table **9**. Coded equations can provide the prediction of the response based on factors that have been considered and identify the relative impact of factors by comparing the factor coefficient. The designed factors were the micro POFA replacement rate denoted as Factor A, the nano POFA replacement rate denoted as Factor B, and the grinding cycles of nano POFA denoted as Factor C. The corresponding responses were the compressive strength of mortar at the curing ages of 7, 28, and 90 days. Different order polynomial was selected in each response surface model to

meet the level of significance and fit the data with a good correlation coefficient. Hence, the 7-day compressive strength (CS) response surface model was a two-factor interaction (2FL) process order, while the 28- and 90-day CS response surface models were in the quadratic process order.

Analysis of variance (ANOVA) was implemented in each response surface model for interpreting the data, as shown in Tables **10** - **12**. Results have been further expressed in terms of the sum of square, degree of freedom, mean square, F-value, and p-value. All three response surface models demonstrated an F-value of 20.25, 11.67, and 15.14, which indicated these models to be significant. In addition, the p-value model term played an important role in determining the significance of each factor, where a value lower than 0.05 was indicated as significant, and vice versa, a value greater than 0.1000 was not considered significant. In all three response surface models, Factor A and B were significant model terms, while the 7-day CS model had an additional significant model term as Factor AB; however, an additional significant Factor A^2 was observed in 28- and 90-day CS models. The significant impact of Factors A and B is aforementioned and has been proven in these response surface models. Moreover, at the p-value of Factor C, the grinding cycle of nano POFA was found to decrease near to significant level at late curing age compared to 7- and 28-day curing ages. Smaller particle sizes of SCM particles exhibited better pozzolanic reactivity and enhanced nucleation sites for the reaction [51]. However, due to the small dosage of nano POFA as well as the small deviation of particle size between three nano POFAs, the impact of Factor C was more significant at the later curing age.

Table 9. Prediction equation of mortar's compressive strength at each curing age in terms of coded factors.

Response	Compressive Strength at 7 Days	Compressive Strength at 28 Days	Compressive Strength at 90 Days
Constant	+38.67	+49.18	+54.84
Factor A	-3.43	-3.75	-3.29
Factor B	+0.9350	+1.33	+0.8433
Factor C	-0.3550	+0.2072	+0.5750
Factor AB	-1.61	+0.9650	+0.0308
Factor AC	+0.1083	+0.5050	+0.4000
Factor BC	+0.1150	-0.7708	+0.0892
A^2	-	+3.38	+1.83
B^2	-	-1.35	-1.14
C^2	-	+0.5628	+1.03

Table 10. ANOVA analysis of the 7-day compressive strength response surface model in 2FL process order.

Source	Sum of Square	DF	Mean Square	F-value	p-value
Model	261.76	6	43.63	20.25	0.0001
A	212.32	1	212.32	98.53	0.0001
B	15.74	1	15.74	7.30	0.0137
C	2.27	1	2.27	1.05	0.3171
AB	31.14	1	31.14	14.45	0.0011
AC	0.1408	1	0.1408	0.0654	0.8008
BC	0.1587	1	0.1587	0.0736	0.7889
Residual	43.10	20	2.15	-	-
Cor total	304.85	26	-	-	-

Table 11. ANOVA analysis of the 28-day compressive strength response surface model in the quadratic process order.

Source	Sum of Square	DF	Mean Square	F-value	p-value
Model	388.03	9	43.11	11.67	0.0001
A	252.68	1	252.68	68.38	0.0001
B	31.95	1	31.95	8.65	0.0091
C	0.7729	1	0.7729	0.2092	0.6532
AB	11.17	1	11.17	3.02	0.1001
AC	3.06	1	3.06	0.8282	0.3755
BC	7.13	1	7.13	1.93	0.1827
A^2	68.46	1	68.46	18.53	0.0005
B^2	10.92	1	10.92	2.95	0.1038

(Table 11) contd.....

Source	Sum of Square	DF	Mean Square	F-value	p-value
C^2	1.90	1	1.90	0.5143	0.4830
Residual	62.81	17	3.69	-	-
Cor total	450.85	26	-	-	-

Table 12. ANOVA analysis of the 90-day compressive strength response surface model in the quadratic process order.

Source	Sum of Square	DF	Mean Square	F-value	p-value
Model	249.50	9	27.72	15.14	0.0001
A	194.50	1	194.50	106.25	0.0001
B	12.80	1	12.80	6.99	0.0170
C	5.95	1	5.95	3.25	0.0891
AB	0.0114	1	0.0114	0.0062	0.9380
AC	1.92	1	1.92	1.05	0.3201
BC	0.0954	1	0.0954	0.0521	0.8221
A^2	20.03	1	20.03	10.94	0.0042
B^2	7.81	1	7.81	4.27	0.0544
C^2	6.37	1	6.37	3.48	0.0794
Residual	31.12	17	1.83	-	-
Cor total	280.62	26	-	-	-

Table 13. Response surface model fit statistics.

Response	7 days Compressive Strength	28 days Compressive Strength	90 days Compressive Strength
Coefficient of determination, R^2	0.8586	0.8607	0.8891
Adjusted R^2	0.8162	0.7869	0.8304
Predicted R^2	0.7081	0.6904	0.6965
Standard deviation	1.47	1.92	1.35
Mean	38.67	50.90	55.99
Adequate precision	14.1426	11.0446	11.8960
Predicted residual error sum of square	88.99	139.57	85.16

Table 14. Optimizing criteria for the maximum 7-, 28-, and 90-day compressive strength.

Criteria	Optimization Target	Lower Limit	Upper Limit
Micro POFA (%), A	In range	10	30
Nano POFA (%), B	In range	1	3
Grinding cycles, C	In range	50,000	110,000
Compressive strength (MPa) at 7 days	Maximize	40.74	46.37
Compressive strength (MPa) at 28 days	Maximize	56.93	57.77
Compressive strength (MPa) at 90 days	Maximize	59.62	62.36

The coefficient of determination, R^2 of each response surface model is presented in Table **13** for testing the models' adequacy, fitness, and consistency. A model having an R^2 value greater than 0.8 and closer to 1 can be considered a good fit with respect to the experiment data [52, 53]. All three models had an R^2 value greater than 0.8 and showed that around 14.14%, 13.93%, and 11.09% of data did not closely link to the model. Besides that, the difference between adjusted R^2 and predicted R^2 was less than 0.2, which showed both terms to be reasonably in agreement with each other [52, 54]. Last but not least, the adequate precision of three response surface models was greater than 4, which is an adequate signal-to-noise ratio; thus, these models can be used to navigate the design space.

3.3.2. Numerical Optimization

The RSM numerical optimization could suggest an optimum input factor to achieve the best performance of the response. In this case, the replacement rate of micro POFA, nano POFA, and the grinding cycles were taken into account to conclude the best solution that achieved the maximum compressive strength at 7, 28, and 90 days (Table **14**). As a result, RSM suggested utilizing 10% micro POFA, 2.395% to 3% nano POFA, and the grinding cycle of either 50k cycles or 110k cycles to achieve the maximum compressive strength at

respective curing ages. At the earlier curing age, the 50k cycles nano POFA could improve the cement mixture's compressive strength more efficiently, while the 110k cycles nano POFA based mortar exhibited better performance at late curing age.

CONCLUSION

This paper aimed to evaluate the suitability of using a Los Angeles abrasion machine with a slow grinding speed of 33 rpm with improved grinding parameters to produce nano POFA. Moreover, this research has also attempted to figure out the utilization of nano POFA, having a particle size in the range of 150 nm to 985 nm, as cement replacement in cementitious mixtures. The following can be concluded:

• After being ground in the machine for 50k, 80k, and 110k cycles, the micro POFA was successfully reduced to 529 nm, 325 nm, and 103 nm in size. While the specific surface area of the three types of nano POFA was similar, a small increment trend has been observed with decreasing particle size.

• Upon conducting the grinding process for the second time, the LOI values of all nano POFA increased compared to the micro POFA. While a combination of the thermal treatment and mechanical grinding process improved the sum of chemical content (Al_2O_3, SiO_2, and Fe_2O_3) to 75.38%. The crystalline phase of the micro POFA and nano POFA demonstrated no significant changes, but a reduction in the peak intensity was found for the 110k nano POFA compared to the micro POFA. Overall, the XRD showed both POFA to be major in quartz with low crystallinity.

• Increasing nano POFA's dosage led to an increase in the fresh mortar's flowability. This impacted the mortar's fresh properties more than different grinding cycles of nano POFA, where the 110k cycles nano POFA mortar has shown a higher flow diameter than the 50k cycle nano POFA.

• In terms of the hardened properties of POFA-based mortar, the mortar that contained 10% micro and 2 to 3% nano POFA performed the most at all curing ages. Increasing the dosage of micro POFA led to a decrement in the mortar's CS, but the mortars' strength has been improved by using more dosage of nano POFA. The mortar that contained 10% micro and 2-3% nano POFA had a higher relative CS than the control sample with an improvement rate of 7.9, 1.48, and 4.6% at the 7, 28, and 90 days curing age.

• 50k cycles nano POFA-based mortar performed better in terms of CS than other nano POFA at the curing age of 7 days. However, the 110k cycles nano POFA-based mortar had a higher CS at the following curing ages.

• RSM has been used for describing the relationship between the replacement rate of micro POFA, nano POFA, and the different grinding cycles of nano POFA against the compressive strength of mortar at 7, 28, and 90 days with the aid of mathematical equation. All response surface models showed good agreement with the experiment data, where all models' R^2 value was greater than 0.8, while the difference between adjusted and predicted R^2 was less than 0.2.

• Through the numerical optimization, the combination of 10 micro POFA and 2.34% to 3% nano POFA as cement replacement could improve the compressive strength of mortar at all observed curing ages. While the 50k cycles nano POFA-based mortar performed better at 7 days curing age, 110k cycles nano POFA mortar had higher CS at later curing ages.

The use of a low grinding speed LA abrasion machine could produce nano POFA with the proposed grinding parameters. Although a longer time is required to grind the micro POFA to the size of 103 nm, this might make it easier to scale up the production of nano POFA. Concerning the impact of using a nano POFA with particle size ranging from 529 nm to 103 nm, the RSM models showed this factor as insignificant to the replacement rate of micro and nano POFA at all curing ages. It might be due to the low dosage of the nano POFA used in the mix design, improving the mortar's strength at the optimum replacement rate. Hence, using the low dosage of nano POFA with a coarser particle size in the range of 2 to 3% is suggested for the future work to achieve a balance between strength improvement and economic consideration.

LIST OF ABBREVIATIONS

LA abrasion machine	=	Los Angeles abrasion machine
POFA	=	Palm oil fuel ash
RSM	=	Response surface methodology
SCM	=	Supplementary cementitious material
BET analysis	=	Brunauer–Emmett–Teller analysis
LOI value	=	Loss of ignition value
XRF	=	X-ray fluorescence
XRD	=	X-ray diffraction
SEM	=	Scanning electron microscopy
CS	=	Compressive strength
2FL	=	Two-factor interaction

CONSENT FOR PUBLICATION

Not applicable.

AVAILABILITY OF DATA AND MATERIALS

The data used to support the findings of this study will be available from the corresponding author [C.C] upon request.

FUNDING

This work was financially supported by UMPSA Internal Grant (PGRS 220322) and IIUM-UMP Sustainable Research Collaboration Grant (RDU223222).

CONFLICT OF INTEREST

The authors declare no conflict of interest, financial or otherwise.

ACKNOWLEDGEMENTS

The authors acknowledge the financial support provided by UMPSA Internal Grant (PGRS 220322) and IIUM-UMP Sustainable Research Collaboration Grant (RDU223222).

REFERENCES

[1] C.D. Dinga, and Z. Wen, "China's green deal: Can China's cement industry achieve carbon neutral emissions by 2060?", *Renew. Sustain. Energy Rev.,* vol. 155, p. 111931, 2022. [http://dx.doi.org/10.1016/j.rser.2021.111931]

[2] X. Cao, Z. Wen, X. Zhao, Y. Wang, and H. Zhang, "Quantitative

assessment of energy conservation and emission reduction effects of nationwide industrial symbiosis in China", *Sci. Total Environ.,* vol. 717, p. 137114, 2020.
[http://dx.doi.org/10.1016/j.scitotenv.2020.137114] [PMID: 32062260]

[3] K.L. Ting, K. Vallyutham, C.H. Phoon, P.K. Manokaran, and C.C. Lim, "Prospect of CO2 sequestration in Malaysia cement industry", *IOP Conference Series: Earth and Environmental Science,* , 2023p. 012049
[http://dx.doi.org/10.1088/1755-1315/1135/1/012049]

[4] Y. Guo, L. Luo, T. Liu, L. Hao, Y. Li, P. Liu, and T. Zhu, "A review of low-carbon technologies and projects for the global cement industry", *J. Environ. Sci.,* vol. 136, pp. 682-697, 2024.
[http://dx.doi.org/10.1016/j.jes.2023.01.021]

[5] G. Cordoba, and E.F. Irassar, "Carbon footprint of reinforced concrete columns with and without supplementary cementitious materials", *Int. J. Life Cycle Assess.,* vol. 28, no. 7, pp. 800-812, 2023.
[http://dx.doi.org/10.1007/s11367-023-02182-w]

[6] J.H.A. Rocha, R.D. Toledo Filho, and N.G. Cayo-Chileno, "Sustainable alternatives to CO2 reduction in the cement industry: A short review", *Mater. Today Proc.,* vol. 57, pp. 436-439, 2022.
[http://dx.doi.org/10.1016/j.matpr.2021.12.565]

[7] J.Y. Richard Liew, M-X. Xiong, and B-L. Lai, *Chapter 07 - Special considerations for high strength materials,* 2021.
[http://dx.doi.org/10.1016/B978-0-12-823396-2.00011-3]

[8] R.B. Holland, K.E. Kurtis, and L.F. Kahn, "7 - Effect of different concrete materials on the corrosion of the embedded reinforcing steel", In: A. Poursaee, Ed., *Corrosion of Steel in Concrete Structures.,* Woodhead Publishing: Oxford, 2016, pp. 131-147.
[http://dx.doi.org/10.1016/B978-1-78242-381-2.00007-9]

[9] S. Park, S. Wu, Z. Liu, and S. Pyo, "The role of supplementary cementitious materials (SCMs) in ultra high performance concrete (UHPC): A review", *Materials,* vol. 14, no. 6, p. 1472, 2021.
[http://dx.doi.org/10.3390/ma14061472] [PMID: 33802943]

[10] H.M. Hamada, B.S. Thomas, F.M. Yahaya, K. Muthusamy, J. Yang, J.A. Abdalla, and R.A. Hawileh, "Sustainable use of palm oil fuel ash as a supplementary cementitious material: A comprehensive review", *J. Build. Eng.,* vol. 40, p. 102286, 2021.
[http://dx.doi.org/10.1016/j.jobe.2021.102286]

[11] B.S. Thomas, S. Kumar, and H.S. Arel, "Sustainable concrete containing palm oil fuel ash as a supplementary cementitious material-a review", *Renew. Sustain. Energy Rev.,* vol. 80, pp. 550-561, 2017.
[http://dx.doi.org/10.1016/j.rser.2017.05.128]

[12] C. Beng Wei, R. Othman, C. Yee Ying, R. Putra Jaya, D. Shu Ing, and S. Ali Mangi, "Properties of mortar with fine eggshell powder as partial cement replacement", *Mater. Today Proc.,* vol. 46, pp. 1574-1581, 2021.
[http://dx.doi.org/10.1016/j.matpr.2020.07.240]

[13] P.J. Ramadhansyah, A.W. Mahyun, M.Z.M. Salwa, B.H. Abu Bakar, M.A. Megat Johari, and M.H. Wan Ibrahim, "Thermal analysis and pozzolanic index of rice husk ash at different grinding time", *Procedia Eng.,* vol. 50, pp. 101-109, 2012.
[http://dx.doi.org/10.1016/j.proeng.2012.10.013]

[14] S.A. Alabi, and J. Mahachi, "Compressive strength of concrete containing palm oil fuel ash under different curing techniques", *Mater. Today Proc.,* vol. 43, pp. 1969-1972, 2021.
[http://dx.doi.org/10.1016/j.matpr.2020.11.426]

[15] K. Srikanth, D.C.K. Jagarapu, T.V. Das, S.H. Jeelani, and A. Eluru, "Evaluation of the effective mechanical properties of palm oil fuel ash based fiber reinforced concrete", *IOP Conf Ser Mater Sci Eng,* vol. vol. 1136, 2021p. 12041
[http://dx.doi.org/10.1088/1757-899X/1136/1/012041]

[16] A.K. Mali, and P. Nanthagopalan, "Comminution: A supplementation for pozzolanic adaptation of sugarcane bagasse ash", *J. Mater. Civ. Eng.,* vol. 33, no. 12, p. 04021343, 2021.
[http://dx.doi.org/10.1061/(ASCE)MT.1943-5533.0003985]

[17] P. Pormmoon, A. Abdulmatin, C. Charoenwaiyachet, W. Tangchirapat, and C. Jaturapitakkul, "Effect of cut-size particles on the pozzolanic property of bottom ash", *J. Mater. Res. Technol.,* vol. 10, pp. 240-249, 2021.
[http://dx.doi.org/10.1016/j.jmrt.2020.12.017]

[18] W. Nur, F. Binti, and W. Hassan, Mix Design Optimisation and Durability Study of High Performance Concrete Containing Micro and Nano Palm Oil Fuel Ash*,* Doctor of Philosophy, Curtin University, 2019.

[19] W. Le Tang, Department of Civil Engineering Carbonation of Concrete Incorporating High Volume of Micro and Low Volume of Nano Palm Oil Fuel Ash*,* Master of Philosophy (Civil Engineering), Curtin University, 2018.

[20] W.N.F. Wan Hassan, M.A. Ismail, H-S. Lee, M.S. Meddah, J.K. Singh, M.W. Hussin, and M. Ismail, "Mixture optimization of high-strength blended concrete using central composite design", *Constr. Build. Mater.,* vol. 243, p. 118251, 2020.
[http://dx.doi.org/10.1016/j.conbuildmat.2020.118251]

[21] K-W. Wi, "An experimental study on the hydration properties of nano palm oil fuel ash. Hanyang University", Available from: https://repository.hanyang.ac.kr/handle/20.500.11754/125270

[22] M. Samadi, G.F. Huseien, N.H.A.S. Lim, H. Mohammadhosseini, R. Alyousef, J. Mirza, and A.B.A. Rahman, "Enhanced performance of nano-palm oil ash-based green mortar against sulphate environment", *J. Build. Eng.,* vol. 32, p. 101640, 2020.
[http://dx.doi.org/10.1016/j.jobe.2020.101640]

[23] M.W. Hussin, "Long term studies on compressive strength of high volume nano palm oil fuel ash mortar mixes", *J. Teknol.,* vol. 77, no. 16, pp. 15-20, 2015.
[http://dx.doi.org/10.11113/jt.v77.6387]

[24] A.M. Zeyad, B.A. Tayeh, A.M. Saba, and M.A.M. Johari, "Workability, setting time and strength of high-strength concrete containing high volume of palm oil fuel ash", *Open Civ. Eng. J.,* vol. 12, no. 1, pp. 35-46, 2018.
[http://dx.doi.org/10.2174/1874149501812010035]

[25] M.A.A. Rajak, Z.A. Majid, and M. Ismail, "Cement hydration extents for hardened cement paste incorporating nanosized-palm oil fuel ash: A thermal and XRD analysis study", In: *Lecture Notes in Civil Engineering,* Springer Singapore: Singapore, 2020, pp. 61-70.
[http://dx.doi.org/10.1007/978-981-15-1193-6_7]

[26] W.L. Tang, H.S. Lee, V. Vimonsatit, T. Htut, J.K. Singh, W.N.F. Wan Hassan, M.A. Ismail, A.H. Seikh, and N. Alharthi, "Optimization of micro and nano palm oil fuel ash to determine the carbonation resistance of the concrete in accelerated condition", *Materials,* vol. 12, no. 1, p. 130, 2019.
[http://dx.doi.org/10.3390/ma12010130] [PMID: 30609786]

[27] M.A.A. Rajak, Z. Abdul Majid, and M. Ismail, "The effects of nanosized-palm oil fuel ash on early age hydration of hardened cement paste: The microstructure studies", *Journal of Advanced Research in Fluid Mechanics and Thermal Sciences,* vol. 82, no. 2, pp. 87-95, 2021.
[http://dx.doi.org/10.37934/arfmts.82.2.8795]

[28] S. Rizal, C.K. Abdullah, N.G. Olaiya, N.A. Sri Aprilia, I. Zein, I. Surya, and H.P.S. Abdul Khalil, "Preparation of palm oil ash nanoparticles: Taguchi optimization method by particle size distribution and morphological studies", *Appl. Sci.,* vol. 10, no. 3, p. 985, 2020.
[http://dx.doi.org/10.3390/app10030985]

[29] H.M. Hamada, A.A. Al-Attar, B. Tayeh, and F.B.M. Yahaya, "Optimizing the concrete strength of lightweight concrete containing nano palm oil fuel ash and palm oil clinker using response surface method", *Case Studies in Construction Materials,* vol. 16, p. e01061, 2022.
[http://dx.doi.org/10.1016/j.cscm.2022.e01061]

[30] M. Adamu, Y.E. Ibrahim, and H. Alanazi, "Evaluating the influence of elevated temperature on compressive strength of date-palm-fiber-reinforced concrete using response surface methodology", *Materials,* vol. 15, no. 22, p. 8129, 2022.
[http://dx.doi.org/10.3390/ma15228129] [PMID: 36431614]

[31] A. Waqar, N. Bheel, H.R. Almujibah, O. Benjeddou, M. Alwetaishi, M. Ahmad, and M.M.S. Sabri, "Effect of Coir Fibre Ash (CFA) on the strengths, modulus of elasticity and embodied carbon of concrete using response surface methodology (RSM) and optimization", *Results in Engineering,* vol. 17, p. 100883, 2023.
[http://dx.doi.org/10.1016/j.rineng.2023.100883]

[32] A.A. Shahmansouri, M. Nematzadeh, and A. Behnood, "Mechanical properties of GGBFS-based geopolymer concrete incorporating natural zeolite and silica fume with an optimum design using response surface method", *J. Build. Eng.,* vol. 36, p. 102138, 2021.
[http://dx.doi.org/10.1016/j.jobe.2020.102138]

[33] Z. Li, D. Lu, and X. Gao, "Optimization of mixture proportions by statistical experimental design using response surface method - A review", *J. Build. Eng.,* vol. 36, p. 102101, 2021.
[http://dx.doi.org/10.1016/j.jobe.2020.102101]

[34] A.Y. Goren, Y.K. Recepoğlu, and A. Khataee, "Language of response surface methodology as an experimental strategy for electrochemical wastewater treatment process optimization", In: M. Asadnia, A. Razmjou, and A. Beheshti, Eds., *Artificial Intelligence and Data*

Science in Environmental Sensing., Academic Press, 2022, pp. 57-92. [http://dx.doi.org/10.1016/B978-0-323-90508-4.00009-5]

[35] H. Hamada, B. Tayeh, F. Yahaya, K. Muthusamy, and A. Al-Attar, "Effects of nano-palm oil fuel ash and nano-eggshell powder on concrete", *Constr. Build. Mater.,* vol. 261, p. 119790, 2020. [http://dx.doi.org/10.1016/j.conbuildmat.2020.119790]

[36] K. Wi, H.S. Lee, S. Lim, H. Song, M.W. Hussin, and M.A. Ismail, "Use of an agricultural by-product, nano sized Palm Oil Fuel Ash as a supplementary cementitious material", *Constr. Build. Mater.,* vol. 183, pp. 139-149, 2018. [http://dx.doi.org/10.1016/j.conbuildmat.2018.06.156]

[37] H.M. Hamada, F.M. Yahaya, K. Muthusamy, G.A. Jokhio, and A.M. Humada, "Fresh and hardened properties of palm oil clinker lightweight aggregate concrete incorporating Nano-palm oil fuel ash", *Constr. Build. Mater.,* vol. 214, pp. 344-354, 2019. [http://dx.doi.org/10.1016/j.conbuildmat.2019.04.101]

[38] A.M. Zeyad, M.A. Megat Johari, B.A. Tayeh, and M.O. Yusuf, "Pozzolanic reactivity of ultrafine palm oil fuel ash waste on strength and durability performances of high strength concrete", *J. Clean. Prod.,* vol. 144, pp. 511-522, 2017. [http://dx.doi.org/10.1016/j.jclepro.2016.12.121]

[39] A.S.M.A. Awal, and I.A. Shehu, "Evaluation of heat of hydration of concrete containing high volume palm oil fuel ash", *Fuel,* vol. 105, pp. 728-731, 2013. [http://dx.doi.org/10.1016/j.fuel.2012.10.020]

[40] H.J. Chen, N.H. Shih, C.H. Wu, and S.K. Lin, "Effects of the loss on ignition of fly ash on the properties of high-volume fly ash concrete", *Sustainability,* vol. 11, no. 9, p. 2704, 2019. [http://dx.doi.org/10.3390/su11092704]

[41] Y. Phethany, and P. Julnipitawong, *Effect of LOI of fly ash on properties of concrete.,* Thammasat University, 2017.

[42] R. Alyousef, H. Mohammadhosseini, F. Alrshoudi, M. Md, H. Tahir, Alabduljabbar. , and A.M. Mohamed, "Enhanced performance of concrete composites comprising waste metalised polypropylene fibres exposed to aggressive environments", *Crystals,* vol. 10, no. 8, 2020. [http://dx.doi.org/10.3390/cryst10080696]

[43] S. Cheng, K. Ge, T. Sun, Z. Shui, X. Chen, and J.X. Lu, "Pozzolanic activity of mechanochemically and thermally activated coal-series kaolin in cement-based materials", *Constr. Build. Mater.,* vol. 299, p. 123972, 2021. [http://dx.doi.org/10.1016/j.conbuildmat.2021.123972]

[44] H.N. Kim, J.W. Kim, M.S. Kim, B.H. Lee, and J.C. Kim, "Effects of ball size on the grinding behavior of talc using a high-energy ball mill", *Minerals,* vol. 9, no. 11, p. 668, 2019. [http://dx.doi.org/10.3390/min9110668]

[45] W.N.F.W. Hassan, M.A. Ismail, H. Lee, M.W. Hussin, M. Ismail, and J.K. Singh, "Utilization of nano agricultural waste to improve the workability and early strength of concrete", *International Journal of Sustainable Building Technology and Urban Development,* vol. 8, no. 4, pp. 316-331, 2017. [http://dx.doi.org/10.22712/susb.20170030]

[46] W.N.F.W. Hassan, M. Ismail, M.A. Ismail, H.S. Lee, and M.W. Hussin, "Fresh and hardened properties of high-performance concrete utilising micro and nano palm oil fuel ash", *Malays. Constr. Res. J.,* p. 36, 2020.

[47] H.M. Hamada, A.A. Al-attar, F.M. Yahaya, K. Muthusamy, B.A. Tayeh, and A.M. Humada, "Effect of high-volume ultrafine palm oil fuel ash on the engineering and transport properties of concrete", *Case Studies in Construction Materials,* vol. 12, p. e00318, 2020. [http://dx.doi.org/10.1016/j.cscm.2019.e00318]

[48] A.M. Zeyad, M.A. Megat Johari, A. Abadel, A. Abutaleb, M.J.A. Mijarsh, and A. Almalki, "Transport properties of palm oil fuel ash-based high-performance green concrete subjected to steam curing regimes", *Case Studies in Construction Materials,* vol. 16, p. e01077, 2022. [http://dx.doi.org/10.1016/j.cscm.2022.e01077]

[49] N.H.A.S. Lim, M.A. Ismail, H.S. Lee, M.W. Hussin, A.R.M. Sam, and M. Samadi, "The effects of high volume nano palm oil fuel ash on microstructure properties and hydration temperature of mortar", *Constr. Build. Mater.,* vol. 93, pp. 29-34, 2015. [http://dx.doi.org/10.1016/j.conbuildmat.2015.05.107]

[50] H. Zhang, B. He, B. Zhao, and P. JM Monteiro, "Using diatomite as a partial replacement of cement for improving the performance of recycled aggregate concrete (RAC)-Effects and mechanism", *Constr. Build. Mater.,* vol. 385, p. 131518, 2023. [http://dx.doi.org/10.1016/j.conbuildmat.2023.131518]

[51] M.C.G. Juenger, and R. Siddique, "Recent advances in understanding the role of supplementary cementitious materials in concrete", *Cement Concr. Res.,* vol. 78, pp. 71-80, 2015. [http://dx.doi.org/10.1016/j.cemconres.2015.03.018]

[52] M. Adamu, M.L. Marouf, Y.E. Ibrahim, O.S. Ahmed, H. Alanazi, and A.L. Marouf, "Modeling and optimization of the mechanical properties of date fiber reinforced concrete containing silica fume using response surface methodology", *Case Studies in Construction Materials,* vol. 17, p. e01633, 2022. [http://dx.doi.org/10.1016/j.cscm.2022.e01633]

[53] M. Adamu, P. Trabanpruek, P. Jongvivatsakul, S. Likitlersuang, and M. Iwanami, "Mechanical performance and optimization of high-volume fly ash concrete containing plastic wastes and graphene nanoplatelets using response surface methodology", *Constr. Build. Mater.,* vol. 308, p. 125085, 2021. [http://dx.doi.org/10.1016/j.conbuildmat.2021.125085]

[54] M. Adamu, K.O. Ayeni, S.I. Haruna, Y.E.H. Ibrahim Mansour, and S. Haruna, "Durability performance of pervious concrete containing rice husk ash and calcium carbide: A response surface methodology approach", *Case Studies in Construction Materials,* vol. 14, p. e00547, 2021. [http://dx.doi.org/10.1016/j.cscm.2021.e00547]